https://doi.org/10.1016/j.engstruct.2020.111184

Testing, finite element analysis and design of high strength steel RHS T-joints

Xiaoyi Lan[a,1,*], Tak-Ming Chan[b], Ben Young[b]

[a] School of Civil and Environmental Engineering, Nanyang Technological University, Singapore

[b] Dept. of Civil and Environmental Engineering, The Hong Kong Polytechnic University, Hong Kong, China

[1] Formerly, Dept. of Civil and Environmental Engineering, The Hong Kong Polytechnic University, Hong Kong, China

*xiaoyi.lan@connect.polyu.hk

Abstract: This paper investigates the structural behaviour of high strength steel (HSS) rectangular hollow section (RHS) T-joints under brace axial compression. Seven fabricated RHS T-joints which were composed of built-up steel tubes with a measured yield stress of 907 MPa were tested. Extensive finite element simulations on the fabricated RHS T-joints covering a wide range of geometric parameters and steel grades ranging from S460 to S960 were conducted. The chord face plastification, chord side wall failure and a combination of these two failure modes in the fabricated RHS T-joints were examined. The effects of material softening in the heat affected zones (HAZ) on the joint behaviour and influences of the steel grade, brace to chord width ratio (β) and chord width to wall thickness (2γ) on the suitability of the CIDECT strength equations for the fabricated RHS T-joints were evaluated. The deformation capacity and ductility of test specimens are shown to be reasonably sufficient. The effect of HAZ on the initial stiffness of the fabricated RHS T-joints is insignificant. The HAZ can lower the joint strength more significantly for medium β ratio; however, the joint strength reduction is less pronounced than the material strength reduction. The CIDECT strength prediction for chord face plastification is more unconservative for higher steel grade, larger 2γ ratio and smaller β ratio and becomes unduly conservative for the combined failure modes and chord side wall failure. It is suggested that $0.4\leq\beta\leq0.85$ and $2\gamma\leq60\beta$-1 for chord face plastification to allow for more effective use of HSS and corresponding reasonably conservative strength equations were proposed. Simplified strength equations which are based on an analytical model of plate buckling were proposed for chord side wall failure in the fabricated RHS T-joints with β=1.0 and are also applicable for cold-formed steel RHS T-joints. A linear interpolation approach using the proposed strength equations at β=0.85 and β=1.0 is recommended for the combined failure modes in the

fabricated RHS T-joints with $0.85<\beta<1.0$.

Keywords: Design; Heat affected zone; High strength steel; Rectangular hollow section; T-joint

1. Introduction

High strength steel (HSS) with nominal yield stresses higher than 450 MPa features with advantageous strength-to-weight ratios. It has become readily available because of the rapid advancement of steel production technologies e.g. quenching and tempering (QT), thermo-mechanical controlled processing (TMCP) and direct quenching (DQ) [1]. Tubular structures are widely used in the infrastructure sector such as buildings, bridges, transmission towers and offshore platforms. The application of HSS in tubular structures can reduce the member sizes and subsequent costs of fabrication, transportation and construction. The lower consumption of steel materials can also contribute to the resource-saving, carbon footprint reduction and thus the sustainable development of the infrastructure sector. Design rules for HSS tubular members have been proposed (e.g. Lan et al. [2, 3]); however, research and design guidance for the critical component of HSS tubular joints in HSS tubular structures remain limited.

Design guides and codes e.g. the CIDECT design guides [4, 5] and EN 1993-1-8 [6] are available for tubular joints using steel grades up to S355. Additional reduction factors of joint strength are stipulated for the extension of the codified strength equations to the design of tubular joints using higher steel grades. The CIDECT design guides [4, 5] impose a reduction factor of 0.9 and the limitation on the yield stress to 0.8 times the ultimate stress. Likewise, the current Eurocode 3 [6, 7] also requires the application of reduction factors of 0.9 for steel grades beyond S355 up to S460 and 0.8 for steel grades greater than S460 up to S700. However, the suitability of such design rules for all HSS tubular joints remains controversial and has been re-examined in recent years. Research advances of HSS circular hollow section (CHS) tubular joints have been mostly made for HSS CHS X- and T-joints (e.g. Puthli et al. [8], Lee et al. [9] and Lan et al. [10-13]) and were summarised by Lan and Chan [1]. The recent investigations on HSS rectangular hollow section (RHS) joints are reviewed herein.

Becque and Wilkinson [14] found that the test joint strengths of axially loaded RHS T- and X-joints with a nominal yield stress of 450 MPa are higher than the CIDECT nominal strengths without using the reduction factor for chord face plastification and chord side wall failure except for brittle failure modes of chord punching shear and brace effective width failure. Havula et al. [15] reported that the test in-plane moment resistances of RHS T-joints using S420, S500 and S700 which failed by chord face plastification exceed the Eurocode design strengths without using the reduction factors except for the butt-weld T-joints and the S700 T-joints with small fillet welds. Feldmann et al. [16] examined the structural behaviour of axially loaded S500, S700 and S960 steel RHS X- and K-joints. It is found that the test ultimate loads generally exceed the Eurocode design strengths using the reduction factors. Pandey and Young [17-19] tested the S900 and S960 RHS X- and T-joints under brace axial compression, and found that the Eurocode and CIDECT nominal strength predictions without using the reduction factors are unconservative for chord face plastification and conservative for chord side wall failure. Kim et al. [20] reported that the test joint strengths of chord face plastification and chord side wall failure in RHS X-joints with a nominal yield stress of 650 MPa and under brace axial compression are higher than the Eurocode nominal strengths without using the reduction factor. It is noteworthy that the aforementioned research has been focused on cold-formed and hot-finished HSS tubular joints. However, studies for fabricated HSS tubular joints using built-up steel tubes which are preferred in heavy-weight tubular structures remain limited. Lan et al. [21] investigated the chord face plastification, chord side wall failure and a combination of these two failure modes in the fabricated RHS X-joints using S460 up to S960 and under brace axial compression. Design rules were proposed for the X-joints.

This study assesses the structural performance of fabricated RHS T-joints using S460 up to S960 steel and under brace axial compression. Seven fabricated RHS T-joints with a measured yield stress of 907 MPa were tested and the load-deformation curves of test specimens were recorded. A validated finite element (FE) model was developed and employed to conduct extensive FE simulations. The effects of heat affected zones (HAZ) and the structural performance of the fabricated HSS RHS T-joints were examined. The CIDECT strength equations were assessed. Design rules were proposed for the fabricated HSS RHS T-joints using S460 up to S960 steel.

2. Experimental investigation

2.1. Test specimens

Tests were carried out on seven fabricated RHS T-joints using built-up steel tubes and under brace axial compression. Fig. 1 illustrates the configuration and notations of the fabricated RHS T-joints, in which the full penetration butt weld at the tube corner was used to weld four steel plates into the steel tubes and the fillet weld at the brace-chord intersection was adopted to assemble the steel tubes into the joint specimens. Table 1 summarises the measured dimensions of the test specimens. The examined brace to chord width ratio (β) varied from 0.50 to 0.82 and chord width to wall thickness ratio (2γ) ranged from 19.5 to 49.1. One parental HSS steel plate was used to fabricate the steel tubes and the measured brace and chord wall thickness was 6.14 mm. The angle between the brace and chord members (θ) was 90°. The nominal chord length (L_0) was $6b_0$+90 mm, and the nominal brace length (L_1) was $3b_1$ to avoid the brace flexural buckling [22].

A Chinese Q890 HSS plate manufactured by the QT technique was used to fabricate the steel tubes in this project. The nominal yield stress and carbon equivalent value (CEV) of the parental steel plate were 890 MPa and 0.56%. The material properties of this steel plate were reported by Lan et al. [21] and the measured elastic modulus (E), static yield stress (f_y), static ultimate stress (f_u) and ultimate strain at static ultimate stress (ε_u) were 207 GPa, 907 MPa, 1016 MPa and 5.1%, respectively. Gas metal arc welding (GMAW) was employed to fabricate the steel tubes and to assemble the joint specimens. The full penetration butt weld and fillet weld were designed in line with AWS D1.1/D1.1M [23]. Table 1 shows the measured dimensions of the reinforcement of butt welds (b_w and h_w, see Fig. 1) and the weld leg size of fillet welds (w). The typical values of f_y and f_u of the filler wire used for welding were 930 MPa and 980 MPa, respectively [21]. A robotic welding machine was employed to achieve a consistent and low heat input of 0.38 kJ/mm, and the values of current, voltage and welding speed were 150A, 16V and 300 mm/min. The welding of HSS is currently not covered in the welding codes such as AWS D1.1/D1.1M [23] and thus the welding parameters and procedures suggested by the SSAB Welding Handbook [24] were employed.

2.2. Test set-up and procedures

Fig. 2 illustrates the test set-up adopted for the fabricated RHS T-joint specimens. The axial compression at the brace end was applied using a servo-controlled hydraulic testing machine. The chord member of the RHS T-joint sat on a pair of rollers through two bearing plates with the width of 120 mm along the chord axial direction and the rollers were placed on rigid supports. Table 1 shows the distance between the centre of two rollers (L_s) which was taken as $3h_0+h_1+120$ mm in tests, where h_0 and h_1 are the nominal chord and brace height, respectively, and 120 mm is the bearing plate width. The values of L_s were determined in accordance with the minimum distance between the bearing plates for the interior one-flange loading case of web crippling stipulated by AISI S100 [25]. The four vertical bolts were initially loosened and therefore the ball bearing which can self-adjust according to the flat profile of the brace end plate could rotate freely. A small preload of 4 kN was then applied by driving the specimens upwards using the actuator of the testing machine hidden below the floor, and thus any possible gaps between the brace end plate and the ball bearing could be eliminated. The vertical bolts were afterwards tightened to lock the position of the ball bearing to avoid any rotations in the subsequent testing, and consequently pure axial compression was applied to the brace end.

The deformations of the fabricated RHS T-joints were measured by calibrated linear variable displacement transducers (LVDT). The chord face indentation (u) at the chord crown (see Fig. 1) was obtained using the LVDTs No. 1 and No. 2 (see Fig. 2), and the measurement point of the LVDT No. 1 was 12 mm away from the adjacent brace face. The LVDT No. 2 was placed at the mid-span of the chord to obtain global chord bending deflection. The corresponding measurement point was located at the chord corner (see Fig. 2) because the bottom chord face deformed inwards in testing and the bending deflection measured at the chord corner was not affected by the local deformation of the bottom chord face. The chord face indentation was taken as the reading difference between LVDTs No. 1 and No. 2. The chord side wall deformation (v) was measured by the LVDT No. 3 (see Fig. 2) and a rigid plastic plate was attached to the LVDT tip in order to capture the maximum chord side wall deformation in tests.

The testing continued after preloading by driving the actuator ram upwards at a rate of 0.3 mm/min. The tests were paused for two minutes at large deformations to allow for the static drops and to obtain the static load-deformation curves. The applied loading and LVDT readings were recorded, and the tests were terminated when the joint deformations became excessive for safety purposes.

2.3. Test results

The seven T-joint specimens failed by chord face plastification (see Fig. 3). Figs. 4-5 plot the obtained load-deformation curves. Table 2 shows the static strengths of the RHS T-joints (N_{Test}). The joint strength was determined as the peak load or the load at an indentation limit of $3\%b_0$ at the chord crown, whichever occurred earlier [5]. Figs. 4-5 demonstrate that the deformations of test specimens could generally reach at least two times of the CIDECT indentation limit (see Table 2), and brittle fracture failure was not observed at large deformations. The deformation capacity and ductility of the test specimens could be considered as reasonably sufficient. It should be noted that the failure modes in this study were classified in line with the CIDECT design guide [5] i.e. chord face plastification for $\beta \leq 0.85$, chord side wall failure for $\beta=1.0$ and a combination of the two failure modes for $0.85<\beta<1.0$. The CIDECT strength equations for such failure modes are based on conservative analytical models without considering the beneficial effect of fillet welds or butt welds at the brace-chord intersection (see Section 4.1 of this paper). The β ratios of T1 and T2 specimens were 0.80 and 0.82, respectively, approaching the limit of 0.85 and the fillet weld was adopted to assemble the brace and chord into T-joint specimens in tests. Thus, the chord side wall failure also contributed to the failure of the T1 and T2 specimens, and the peak loads occurred before the indentation limit as shown in Figs. 4(a).

3. Finite element analysis

3.1. Finite element model

Finite element (FE) analysis on the fabricated HSS RHS T-joints was performed using ABAQUS [26]. A FE model was constructed and validated against the test results summarised in Section 2.3 of this paper. The measured dimensions (see Table 1) were adopted. Solid elements were adopted to model

the test specimens, i.e. the brace and chord were modelled by the eight-node linear solid element (C3D8R), and the fillet weld and the reinforcement of the chord butt weld were simulated by the ten-node quadratic tetrahedron solid element (C3D10) and the six-node linear wedge solid element (C3D6), respectively. Suitable mesh sizes varying from 5 to 12 mm depending on the chord cross-section sizes were adopted for the brace, chord and reinforcement of chord butt weld, and the mesh size for the fillet weld was 3 mm. Two layers of the C3D8R element were used through the brace and chord wall thickness. The change of the predicted joint strengths resulted from reducing the mesh sizes and increasing the mesh layers is within 2% of the corresponding test strengths.

The true stress and logarithmic plastic strain which were converted from the measured engineering stress and strain in the coupon tests reported by Lan et al. [21] were used. The Poisson's ratio (v) of steel in this study was taken as 0.3. The von-Mises yield criterion and isotropic strain hardening rules were adopted. Fig. 6 shows the employed boundary conditions which were chosen to closely simulate the test set-up described in Section 2.2 of this paper. The degrees of freedom of all nodes at the brace end were coupled to a concentric reference point (RP-1) by using rigid body constraints. All degrees of freedom of the brace reference point were restricted except the brace axial translation. The degrees of freedom of all nodes of each contact surface (i.e. the yellow surface in Fig. 6) of the bottom chord face to the bearing plate were coupled to a reference point (RP-2 and RP-3) where the roller was placed, and only the chord axial translation and chord in-plane rotation of the chord reference point were allowed. The distance between the reference points of RP-2 and RP-3 was L_s as shown in Table 1, and the length of the contact surfaces along the chord axial direction was 120 mm.

Fig. 3 demonstrates that the predicted failure mode of chord face plastification can closely mirror the test observation. Figs. 4-5 show that the FE model can produce reasonably accurate prediction of the load-deformation curves when compared with the test curves. Table 2 summarises the static strengths of the RHS T-joint specimens obtained from the FE simulations (N_{FE}) and tests (N_{Test}). The mean value of N_{FE}/N_{Test} ratio is 0.97 with corresponding COV of 0.063, and thus the FE joint strengths agree well with the test strengths. Therefore, the constructed FE model is capable of producing accurate prediction of the joint behaviours.

3.2. *Effects of heat affected zones*

The heat input of welding can alter the material properties of heat affected zones (HAZ), which mainly depend on the steel material, heat input, welding type and cooling time [21]. Stroetmann et al. [27] found that there was no material softening in the HAZ of QT S690Q and S960Q steel and TMCP S500M steel except for the TMCP S700 steel. Siltanen et al. [28] also reported that the material softening for DQ S960 steel was around 20% while that of QT S960 steel was negligible. The results show that the material softening can be more pronounced for higher steel grades and more significant for TMCP and DQ HSS than QT HSS. Higher heat input can result in larger material strength reduction in the HAZ of HSS [29]. Comprehensive welding guidance is imperatively needed for HSS in order to mitigate the possible adverse effects of the HAZ in HSS structures.

It is significant to examine the effects of material softening of the HAZ on the structural behaviour of fabricated HSS RHS T-joints because the material softening can occur in HSS tubular structures. FE analysis was carried out on the fabricated S960 RHS T-joints because the material softening is less pronounced for lower steel grades [27-29]. Table 3 shows the geometric parameters of the six FE specimens analysed. The joint parameters of specimens T1-1 and T4-1 which are not tabulated in Table 3 are the same as those of the test specimen T1 and T4, respectively. The FE model described in Section 3.1 of this paper was adopted.

Fig. 7 shows the HAZ in the chord of fabricated S960 steel RHS T-joints. The material properties of the base metal used by Lan et al. [21] were adopted herein. The sizes and material softening of the HAZ were determined in line with Lan et al. [11, 21] which were based on the reported test results of HAZ [27-29]. The width and depth of the HAZ at the brace-chord intersection were taken as t_1+w+12 mm and t_0, respectively. It should be noted that the HAZ in the brace was not modelled in this study because brace failure was not observed in the tests and also not the failure mode consider in this study; however, it should be properly modelled for those investigations that focused on brace failure. The reduction of yield stress (f_y) and ultimate stress (f_u) of the HAZ near the weld which is in red colour (see Fig. 7) was taken as 20%, and that of the HAZ far from the weld (in blue colour) was 10%. The ultimate strain at ultimate stress (ε_u) of the HAZ near the weld (in red) was taken as 2.1 times the

241 value of ε_u of S960 base metal in accordance with the test results reported by Javidan et al. [29]. The
242 elastic modulus (E) of the base metal was adopted for the HAZ. Table 4 summarises the material
243 parameters adopted for the RHS T-joints. Fig. 8 depicts the adopted engineering stress-strain curves
244 obtained from the reported stress-strain curve model [30].
245
246 Fig. 9 shows the obtained load-indentation curves of fabricated S960 steel RHS T-joints without and
247 with HAZ. The effect of the material softening in HAZ on the initial stiffness of the T-joints is found
248 to be minor. This is because the initial stiffness is mainly governed by the steel elastic modulus and
249 the joint geometric parameters. This therefore indicates that the effect of HAZ can be neglected when
250 the elastic analysis on HSS tubular structures is performed. However, the HAZ can lower the stiffness
251 and static strength of the fabricated HSS RHS T-joints when inelastic deformations occur. The static
252 strengths of the T-joints without HAZ (N_{u1}) and with HAZ (N_{u2}) are tabulated in Table 3. The joint
253 strength reduction ranges from 6 to 14% for the fabricated S960 steel RHS T-joints. It is more
254 significant for chord face plastification failure in the T-joints with medium β ratio which typically
255 involves the formation of yield lines in the chord faces at the brace-chord intersection. The joint
256 strength reduction resulted from the HAZ is less significant when compared with the pronounced
257 material softening in the HAZ. This is mainly because the stresses of the HAZ which become plastic
258 can redistribute to adjacent regions and the improved yield stress of HSS is under-utilised for the
259 T-joints with smaller β ratio which will be elaborated in Section 4.2 of this paper. The subsequent
260 parametric study is thus conducted without modelling the HAZ. However, conservative strength
261 equations were proposed for the HSS RHS T-joints to consider the possible joint strength reduction
262 which can be up to 14%. It should be noted that suitable welding procedures e.g. those in the SSAB
263 Welding Handbook [24] are recommended to follow in structural applications in order to avoid
264 excessive material softening in welding, for examples, TMCP and DQ HSS.
265
266 *3.3. Parametric study*
267
268 A parametric study on totally 180 fabricated S460, S690 and S960 steel RHS T-joints was carried out,
269 and 10 series of fabricated RHS T-joints (see Table 5) without chord preloads were modelled for each
270 steel grade. The joint parameters cover the brace to chord width ratio (β) from 0.3 to 1.0, the brace

height to chord width ratio (η) from 0.3 to 1.0, and aspect ratio (ζ) of chord height to width from 0.5 to 1.0. For each series, the analysed chord width to wall thickness ratios (2γ) were 15, 20, 25, 30, 35 and 40. The brace and chord wall thickness were the same and the angle between the brace and chord members (θ) was 90°. The brace length (L_1) was set to be b_1+h_1 to avoid the brace flexural buckling and the chord length (L_0) was taken as $2(2\gamma/10)d_0+h_1$ with a minimum of $5d_0+h_1$ where the value of d_0 was taken as the larger of b_0 or h_0. The chord length was determined in line with the minimum distance between the closest chord crown and an open chord end not connected to other members specified in prEN 1993-1-8 [31]; otherwise, the chord end shall be welded to a cap plate for shorter chord length. The adequately long chord length can enable the localised joint deformation to fully develop and thus the joint capacity can be utilised sufficiently. The weld assembling the brace and chord into the joint specimen was modelled in line with the minimum requirements for the butt weld stipulated by AWS D1.1/D1.1M [23].

The material parameters and engineering stress-strain curves (see Fig. 8) adopted by Lan et al. [21] were employed for the FE simulations herein. Table 4 shows the material parameters. The FE model developed in Section 3.1 of this paper was adopted. Four layers of the C3D8R element through the chord wall thickness were employed for $2\gamma<20$ while two element layers were used for $2\gamma\geq20$, and two element layers were adopted for the brace members. Suitable mesh sizes of 20 mm for the brace and chord members and $t_1/6$ for the butt welds were used. The boundary conditions (see Fig. 6) described in Section 3.1 of this paper were employed for the parametric study. The distance between the two reference points at the bottom chord face was taken as $3h_0+h_1+120$ mm, and only the translation along the chord axial direction and the in-plane rotation of the reference points were allowed. All degrees of freedom of the brace reference point were restricted, except for the brace axial translation.

4. Evaluation of design rules

4.1. Current design rules

The IIW recommendations [32, 33] are widely adopted by international design codes and guides for

hot-finished and cold-formed normal strength steel RHS joints. The CIDECT design guide [5] is based on the third edition of IIW recommendations [33] which employs the indentation limit of 3%b_0. The current Eurocode EN 1991-1-8 [6] follows the second edition of IIW recommendations [32] which takes the peak loads as the joint strengths; however, the latest version of Eurocode prEN 1993-1-8 [31] is updated mainly in line with the third edition of IIW recommendations [33]. The background of the third edition of IIW recommendations [33] is elaborated by Wardenier et al. [34]. The representative CIDECT design rules will therefore be subsequently examined.

The CIDECT design strength equations for chord face plastification in normal strength steel RHS T-joints with $\beta \leq 0.85$ and under brace axial compression are as follows [5]:

$$N_{\text{CIDECT}} = Q_{\text{u}} Q_{\text{f}} \frac{f_{\text{y}} t_0^2}{\sin\theta} \tag{1}$$

$$Q_{\text{u}} = \frac{2\eta}{(1-\beta)\sin\theta} + \frac{4}{\sqrt{1-\beta}} \tag{2}$$

$$Q_{\text{f}} = (1-|n|)^C \tag{3}$$

$$C = \begin{cases} 0.6 - 0.5\beta & \text{for } n < 0 \\ 0.1 & \text{for } n \geq 0 \end{cases} \tag{4}$$

$$n = \frac{N_0}{N_{\text{pl},0}} + \frac{M_0}{M_{\text{pl},0}} \tag{5}$$

where Q_{f} is the chord stress function, and n is the chord stress ratio taken as the sum of the ratio ($N_0/N_{\text{pl},0}$) of the chord axial force (N_0) to the chord axial yield capacity ($N_{\text{pl},0}$) and the ratio ($M_0/M_{\text{pl},0}$) of the chord bending moment (M_0) to the chord plastic moment capacity ($M_{\text{pl},0}$). Negative and positive values of n denote chord compression and tension stresses, respectively. It is noted that the CIDECT design strength equations for chord face plastification in the RHS X- and T-joints are the same and based on the yield line model elaborated by Lan et al. [21] which can give lower bound strength prediction for the test joint strengths. Therefore, the strength equations derived from the analytical model were taken as the characteristic strength equations and a partial safety factor γ_{m}=1.0 was adopted to obtain the CIDECT design strength equations (i.e. the analytical strength equations were employed as the design strength equations) [35].

The CIDECT design strength equations for chord side wall failure in normal strength steel RHS T-joints with β=1.0 and under brace axial compression are as follows [5]:

$$N_{\mathrm{CIDECT}} = \frac{f_{\mathrm{k}} t_0}{\sin\theta} b_{\mathrm{w}} Q_{\mathrm{f}} \tag{6}$$

$$b_{\mathrm{w}} = \frac{2h_1}{\sin\theta} + 10t_0 \tag{7}$$

$$f_{\mathrm{k}} = \chi f_{\mathrm{y}} \tag{8}$$

where χ is the buckling reduction factor according to e.g. the EN 1993-1-1 [36] using the relevant column buckling curve and a slenderness (λ) defined by:

$$\lambda = 3.46\left(\frac{h_0}{t_0} - 2\right)\sqrt{\frac{1}{\sin\theta}} \tag{9}$$

It is noted that the CIDECT design strength equations for the chord side wall failure in the RHS T-joints are based on the pin-ended stub column model elaborated by Lan et al. [21], which can give lower bound strength prediction for the test joint strengths. The analytical strength equations were therefore employed as the design strength equations [35]. However, the adopted analytical model neglects the beneficial strain hardening of steel materials and restraint of the chord face and the brace for the chord side wall. A linear interpolation approach using the strength prediction at β=0.85 and β=1.0 is adopted for the combined failure modes in the RHS T-joints with $0.85<\beta<1.0$. The validity ranges of the CIDECT strength equations (Eqs. (1-9)) are $\beta \geq 0.1+0.02\gamma$ but ≥ 0.25, $2\gamma \leq 40$ and $h_0/t_0 \leq 40$.

4.2. Evaluation of the CIDECT design rules

The CIDECT strength prediction (N_{CIDECT}) was assessed against the test strength (N_{Test}) summarised in Table 2 and the FE strength (N_{FE}) obtained in Section 3.3 of this paper. It should be noted that for the analysed test and FE specimens, there were no applied chord preloads in the roller-supported RHS T-joints. However, the global chord bending moment (M_0) at the chord crown resulted from the applied brace axial compression should be considered in the calculation of Q_{f} using Eqs. (3-5). The value of M_0 can be approximated by M_0=0.25N_{f}(L_{s}-h_1), where N_{f} is the joint strength obtained from the tests and FE simulations, L_{s} is the distance between the centre of two roller supports and h_1 is the brace height. The chord stress ratio (n) varied from -0.07 to -0.89 for the test specimens listed in Table

1 and ranged from -0.04 to -1.03 for the FE specimens described in Section 3.3 of this paper. The absolute value of n becomes larger for larger β ratio and smaller 2γ ratio indicating that the global chord bending moment (M_0) becomes more dominating in the failure of roller-supported RHS T-joints. The chord member failure instead of the joint failure occurs for $n \leq -1$, and the curve of chord stress function (Eq. (3)) is very steep in the vicinity of $n=-1$, possibly resulting large deviations between the actual and predicted joint strengths. Therefore, the joint specimens with $n<-0.95$ were excluded in the subsequent analysis.

Fig. 10 illustrates the comparison of CIDECT strength prediction (N_{CIDECT}) with FE strength (N_{FE}) for the fabricated HSS RHS T-joints (Series 1-8 in Table 5). It is shown that the N_{CIDECT}/N_{FE} ratio increases with increasing steel grades and 2γ ratio but with decreasing β ratio when $\beta \leq 0.85$. Such observation coincides with the test results summarised in Table 2. The CIDECT strength equation (Eq. (1)) is independent of 2γ ratio for $\beta \leq 0.85$. The joint strength of specimens T4-T7 in tests (see Table 2) decreases from 333 to 188 kN when 2γ ratio increases from 19.8 to 49.1 which demonstrates the pronounced effect of 2γ ratio. The effects of steel grade, β ratio and 2γ ratio on the N_{CIDECT}/N_{FE} ratio are relatively insignificant when $0.85<\beta<1.0$. The N_{CIDECT}/N_{FE} ratio decreases for larger 2γ ratio and the effect of steel grade is minor when $\beta=1.0$. Table 6 summarizes the mean value and COV of the N_{CIDECT}/N_{FE} ratio. The mean values of the N_{CIDECT}/N_{FE} ratio are 0.95, 0.57 and 0.44 with corresponding COV of 0.237, 0.060 and 0.601 for $0.3 \leq \beta \leq 0.85$, $0.85<\beta<1.0$ and $\beta=1.0$, respectively. It is noted that the RHS T-joints with β and 2γ ratios beyond the CIDECT validity ranges were excluded in the statistical analysis. The CIDECT strength prediction is unconservative for small β ratio and large 2γ ratio when $\beta \leq 0.85$ and becomes unduly conservative for $0.85<\beta \leq 1.0$.

The deformation of the roller-supported RHS T-joints is characterised by the localised deformation at the brace-chord intersection and the global bending deflection of the chord. Fig. 11 shows the representative load-indentation curves of the fabricated HSS RHS T-joints with $2\gamma=30$. It is shown that the joint strength is determined by the load at the CIDECT indentation limit of $3\%b_0$ (i.e. deformation-controlled) for the RHS T-joints with small β ratio (i.e. 0.3 and 0.5) which failed by chord face plastification. The localised joint deformation is largely elastic, and the adopted indentation limit becomes the governing factor limiting the joint strength. This is because the applied

brace axial compression is mainly resisted by the bending action of the chord face and partially by the global bending of the chord, and the peak load is typically higher than the load at the indentation limit due to the membrane action of the chord face and strain hardening of steel materials. The fabricated RHS T-joints with larger β ratio and lower 2γ ratio can resist larger brace loading resulting in higher stresses in the chord face at the indentation limit. The improved yield stress of HSS can thus be utilised more effectively and the corresponding CIDECT strength prediction which is based on the yield line model assuming the formation of yield lines on the chord faces becomes less unconservative for larger β ratio and lower 2γ ratio. Fig. 12 further illustrates the typical yielding patterns of the RHS T-joints with β=0.5 and 2γ=30 at the determined joint strengths (i.e. the indentation limit). The highly strained areas in red colour become plastic. It is shown that extensive yielding occurs in the chord face and the yield lines are in the process of developing at the indentation limit for the S460 steel RHS T-joints; however, the plastic regions are more confined for higher steel grades of S690 and S960. The corresponding CIDECT strength prediction thus becomes more unconservative for higher steel grade.

The brace axial compression of the fabricated RHS T-joints with β ratio approaching or equal to 1.0 (i.e. 0.8 and 1.0) is jointly resisted by the chord side walls and the global bending action of the chord. The corresponding joint strength is strength-controlled taken as the peak load or the load at the indentation limit which is close to the peak load (see Fig. 11(c)-(d)) and is typically governed by the cross-section yielding or plate buckling of the chord side walls. The improved yield stress of HSS can thus be utilised more effectively. The unduly conservative CIDECT strength prediction for the combined failure modes and chord side wall failure is resulted from the adopted pin-ended stub column model which neglects the strain hardening and the restraint of the chord face and the brace for the chord side wall. It is noted that the CIDECT linear interpolation approach was adopted for $0.85<\beta<1.0$.

5. Proposed design rules

5.1. Chord face plastification

The CIDECT strength equation (Eq. (1)) for chord face plastification was modified and extended for

405 the HSS RHS T-joints. The analysis in Section 4.2 of this paper demonstrates that the improved yield
406 stress of HSS cannot be fully utilised for higher steel grade, smaller β ratio and larger 2γ ratio, and the
407 corresponding CIDECT strength prediction is unconservative and scattered. It is thus suggested to
408 tighten the parameter ranges to be $0.4 \le \beta \le 0.85$ and $2\gamma \le 60\beta - 1$ for steel grades ranging from S460 to
409 S960. The suggested ranges of β and 2γ ratios can avoid applying small reduction factors of joint
410 strength to the CIDECT strength equation for the HSS RHS T-joints which largely eliminate the
411 benefits of using HSS.
412
413 The CIDECT strength prediction is generally unconservative for the fabricated HSS RHS T-joints
414 with $0.4 \le \beta < 0.6$ (see Fig. 10) because of the adopted indentation limit and conservative for $0.6 \le \beta \le 0.85$.
415 Strength equations for the fabricated RHS T-joints in steel grades varying from S460 to S960 are
416 proposed as follows:

$$N_{\text{Proposed}} = Q_{\text{y}} Q_{\text{u}} Q_{\text{f}} \frac{f_{\text{y}} t_0^2}{\sin\theta} \tag{10}$$

$$Q_{\text{y}} = \begin{cases} -62 f_{\text{y}} / E + 1.1 & \text{for } 0.4 \le \beta < 0.6 \\ 1.0 & \text{for } 0.6 \le \beta \le 0.85 \end{cases} \tag{11}$$

417 where Q_{y} is the proposed reduction factor of joint strength to account for the under-utilisation of HSS
418 and equals to 0.96, 0.89 and 0.81 for the examined steel grades S460, S690 and S960, respectively,
419 when $0.4 \le \beta < 0.6$. It is noted that $Q_{\text{y}}=1.0$ for the S355 RHS T-joints and the corresponding proposed
420 strength equation (Eq. (10)) is the same as the CIDECT strength equation (Eq. (1)). The validity
421 ranges of the proposed strength equations are $0.4 \le \beta \le 0.85$, $2\gamma \le 60\beta - 1$ but ≤ 40, and $h_0/t_0 \le 40$ for steel
422 grades ranging from S460 and S960.
423
424 The proposed strength equation (Eq. (10)) was assessed against the FE results obtained in this study.
425 The FE specimens with joint parameters beyond the suggested limits were excluded for the analysis.
426 Table 6 summarises the results of statistical analysis for the $N_{\text{Proposed}}/N_{\text{FE}}$ ratio. The mean value of the
427 $N_{\text{Proposed}}/N_{\text{FE}}$ ratio is 0.83 with corresponding COV of 0.155. The proposed strength equation is
428 reasonably conservative for the HSS RHS T-joints in order to consider the possible joint strength
429 reduction resulted from the HAZ.
430

5.2. Chord side wall failure

The analysis discussed in Section 4.2 of this paper shows that the CIDECT strength prediction is overly conservative for chord side wall failure in the fabricated HSS RHS T-joints with β=1.0 mainly because of the inherent drawbacks of the adopted pin-ended stub column model. Lan et al. [21] proposed an analytical model of plate buckling for chord side wall failure in RHS X-joints which can consider the beneficial strain hardening and the restraint of the chord face and the brace for the chord side wall. The strength equations for chord side wall failure in RHS X-joints proposed by Lan et al. [21] are further simplified herein and extended to the design of RHS T-joints failing by chord side wall failure. It is noted that the CIDECT design guide [5] adopts the same strength equations for chord side wall failure in RHS X- and T-joints because of the similar joint behaviours. The strain hardening which is not significant for HSS is neglected to simplify the calculations in this study.

The elastic buckling stress ($f_{cr,Lan}$) of chord side wall in RHS X-joints with θ=90° failing by chord side wall failure which can properly consider the restraint of the chord face and brace for the chord side wall can be obtained from [21]:

$$f_{cr,Lan} = 3.2\frac{\pi^2 E}{12(1-\nu^2)}\left(\frac{t_0}{h_e}\right)^{1.96}\left(\frac{h_0}{h_1}\right)^{0.66} \tag{12}$$

where h_e is the effective buckling length taken as h_0-2t_0 for the fabricated RHS joints with sharp chord corners and h_0 for hot-finished and cold-formed RHS joints with round chord corners. Eq. (12) is also suggested for chord side wall failure in RHS T-joints without the global chord bending resulted from the brace loading. The overall cross-section slenderness (λ_{Lan}) of chord side walls is defined by:

$$\lambda_{Lan} = \sqrt{\frac{f_y}{f_{cr,Lan}}} \tag{13}$$

The base curves for non-slender and slender chord side walls in RHS X-joints proposed by Lan et al. [21] neglecting the strain hardening effect are as follows:

$$\frac{\varepsilon_{csm}}{\varepsilon_y} = \begin{cases} 1.0 & \text{for } \lambda_{Lan} \le 0.68 \\ 0.91\left(1-\dfrac{0.22}{\lambda_{Lan}^{1.60}}\right)\dfrac{1}{\lambda_{Lan}^{1.60}} & \text{for } \lambda_{Lan} > 0.68 \end{cases} \tag{14}$$

where ε_{csm} is the maximum attainable strain in the chord side wall and ε_y is the steel yield strain of the chord. The corresponding maximum attainable stress (f_{csm}) for chord side wall failure in the RHS X-joints can be obtained from:

$$\frac{f_{csm}}{f_y} = \begin{cases} 1.0 & \text{for } \lambda_{Lan} \le 0.68 \\ 0.91\left(1-\frac{0.22}{\lambda_{Lan}^{1.60}}\right)\frac{1}{\lambda_{Lan}^{1.60}} & \text{for } \lambda_{Lan} > 0.68 \end{cases} \quad (15)$$

where the coefficients can be further rounded off and simplified for RHS X- and T-joints as follows:

$$\chi_{Lan} = \frac{f_{csm}}{f_y} = \begin{cases} 1.0 & \text{for } \lambda_{Lan} \le 0.6 \\ 0.8\left(1-\frac{0.2}{\lambda_{Lan}^{1.6}}\right)\frac{1}{\lambda_{Lan}^{1.6}} & \text{for } \lambda_{Lan} > 0.6 \end{cases} \quad (16)$$

The stress ratio of the maximum attainable stress (f_{csm}) to the steel yield stress of the chord (f_y) is taken as the plate buckling reduction factor of the chord side wall (χ_{Lan}) neglecting the strain hardening.

The joint strength for chord side wall failure in RHS X-joints with θ=90° and under brace axial compression ($N_{Proposed}$) can be determined from [21]:

$$N_{Proposed} = \chi_{Lan} f_y t_0 \left(2h_1 + at_0\right) Q_f \quad (17)$$

where the term of at_0 is adopted to consider the load transferred from an alternative load path to the chord side wall through the chord face. It is noted that different values of the coefficient (a) were recommended for non-slender chord side walls in RHS X-joints, i.e. a=8 for fabricated steel RHS X-joints and a=6 for hot-finished and cold-formed steel counterparts [21]. A unified coefficient of a=10 which is the same as that in the CIDECT strength equation (Eq. (7)) is suggested herein for the fabricated, hot-finished and cold-formed steel RHS T-joints and X-joints with θ=90° to be more user-friendly. The validity ranges of the proposed strength equations are $2\gamma \le 40$ and $h_0/t_0 \le 40$, which are the same as the corresponding CIDECT validity ranges.

The performance of the simplified strength equations (Eqs. (12-13) and Eqs. (16-17)) for RHS T-joints was assessed. Table 6 shows that the mean value of the $N_{Proposed}/N_{FE}$ ratio for β=1.0 is 0.89 with corresponding COV of 0.168. The proposed strength equations are reasonably conservative and can consider the possible joint strength reduction resulted from the HAZ. The joint strengths obtained from the CIDECT design guide [5] (N_{CIDECT}) and the proposed method herein ($N_{Proposed}$) were also

compared with the reported test strengths of cold-formed steel RHS T-joints under brace axial compression which failed by chord side wall failure (N_{Test}) as shown in Table 7. The steel elastic modulus of test specimens was not reported by Zhao et al. [37] and was taken as 210 GPa in accordance with EN 1993-1-1 [36]. The bottom chord face of the test specimens [17, 37] was directly placed on a solid flat base and therefore the global chord bending was eliminated (i.e. Q_f=1.0). The mean values of the N_{CIDECT}/N_{Test} ratio and the $N_{Proposed}/N_{Test}$ ratio are 0.51 and 0.99, respectively, with corresponding COV of 0.442 and 0.067. The comparison of test and FE joint strengths (N_f) with the predicted strengths ($N_{f,pred}$) for the cold-formed and fabricated RHS T-joints is illustrated in Fig. 13. It is shown that the CIDECT strength prediction is increasingly conservative for larger chord side wall slenderness; however, the proposed design method can produce much more accurate and consistent strength prediction.

5.3. Combined failure modes

The CIDECT strength prediction is unduly conservative for the combined failure modes in the RHS T-joints with $0.85<\beta<1.0$ as discussed in Section 4.2 of this paper. This is mainly because the CIDECT strength prediction is overly conservative for β=1.0 and the CIDECT linear interpolation approach is adopted for $0.85<\beta<1.0$. The proposed strength equations for $\beta\leq0.85$ and β=1.0 are reasonably accurate and thus the CIDECT linear interpolation approach is also recommended for $0.85<\beta<1.0$. Table 6 shows that the mean value of the $N_{Proposed}/N_{FE}$ ratio is 0.85 with corresponding COV of 0.041. This thus demonstrates that the linear interpolation is also applicable for the fabricated RHS T-joints with $0.85<\beta<1.0$. It should be noted that conservative design rules were proposed for $0.85<\beta<1.0$ in order to consider the possible joint strength reduction resulted from the HAZ as discussion in Section 3.2 of this paper.

5.4. Determination of design strengths

It is noted that the IIW recommendations [32, 33] adopted a two-step procedure to convert the mean strength equation ($N_{u,m}$) based on test and FE results to the design strength equation ($N_{u,Rd}$). The mean strength equation was firstly converted to the characteristic strength equation ($N_{u,k}$) by considering the

scatter of test results. The design strength equation was then derived from the characteristic strength equation divided by a suitable partial safety factor. The CIDECT analytical models described in Section 4.1 of this paper can provide lower bound strength prediction for test specimens of RHS T-joints [35], and thus the analytical equations derived are adopted as the characteristic strength equations. The deformation capacity and ductility of normal strength steel RHS T-joints is found to be sufficient, and therefore a partial safety factor of 1.0 is adopted to obtain the design strength equations i.e. the analytical strength equations are employed as the design strength equations [35].

The IIW procedure is adopted herein to obtain the design strength equations for the fabricated HSS RHS T-joints. The proposed strength equations which are based on theoretical models are shown to produce reasonably conservative and consistent strength prediction for the RHS T-joints (see Table 6) and thus can be used as the characteristic strength equations. The tests summarised in Table 1 have demonstrated the sufficient deformation capacity and ductility of the HSS test specimens (see Figs. 4-5). A partial safety factor of 1.0 is thus suggested for the HSS RHS T-joints, and the proposed strength equations can be adopted as the design strength equations. It is noted that the validity range of 2γ ratio of the proposed strength equations is suggested to be tightened for chord face plastification in the fabricated RHS T-joints with small β ratio in order to allow for more effective use of HSS. Reinforcing methods can be adopted in HSS RHS joints for the use of commercially available HSS RHS tubes with 2γ ratio beyond the recommended limits, e.g. grouting concrete [38] and welding internal ring stiffeners [39, 40] and external stiffeners [41], and related research is needed.

6. Conclusions

The structural behaviour and static strength of HSS RHS T-joints under brace axial compression were investigated through tests and FE analysis. Seven fabricated RHS T-joints with a measured steel yield stress of 907 MPa were tested, and extensive FE simulations on the fabricated RHS T-joints covering a wide range of geometric parameters and steel grades ranging from S460 to S960 were conducted. The chord face plastification, chord side wall failure and a combination of these two failure modes in the fabricated RHS T-joints were examined. The effects of HAZ on the joint behaviour and influences of the steel grade, β ratio and 2γ ratio on the suitability of the CIDECT strength equations for the

fabricated HSS RHS T-joints were evaluated. Design rules were proposed for the RHS T-joints.

(1) The test specimens failed by chord face plastification. The joint deformation could reach at least two times of the CIDECT indentation limit, and brittle fracture failure was not observed in tests. The deformation capacity and ductility of test specimens were reasonably sufficient.

(2) The effect of HAZ on the initial stiffness of the fabricated HSS RHS T-joints is insignificant. The material softening in HAZ can lower the joint strength more significantly for medium β ratio; however, the joint strength reduction is less pronounced than the material softening.

(3) The CIDECT strength prediction for chord face plastification is more unconservative for higher steel grade, larger 2γ ratio and smaller β ratio and becomes unduly conservative for the combined failure modes and chord side wall failure.

(4) HSS cannot be fully utilised in chord face plastification of the fabricated RHS T-joints with small β ratio and large 2γ ratio because of the adopted CIDECT indentation limit. The CIDECT strength prediction for the combined failure modes and chord side wall failure is unduly conservative mainly due to the adopted pin-ended stub column model neglecting the restraint of the brace and chord face for the chord side wall.

(5) It is suggested that $0.4 \leq \beta \leq 0.85$ and $2\gamma \leq 60\beta - 1$ for chord face plastification in the fabricated RHS T-joints in order to allow for effective use of HSS and corresponding reasonably conservative strength equations were proposed.

(6) Simplified strength equations which are based on an analytical model of plate buckling were proposed for chord side wall failure in the fabricated RHS T-joints with $\beta=1.0$ and are also applicable for cold-formed steel RHS T-joints.

(7) The CIDECT linear interpolation using the proposed strength equations at $\beta=0.85$ and $\beta=1.0$ is recommended for the combined failure modes in the fabricated RHS T-joints with $0.85<\beta<1.0$.

Table 1

Measured dimensions of fabricated HSS RHS T-joint specimens.

Specimen	b_0 (mm)	h_0 (mm)	L_0 (mm)	b_1 (mm)	h_1 (mm)	L_1 (mm)	b_w (mm)	h_w (mm)	w (mm)	L_s (mm)
T1	121.7	122.9	808	96.8	98.3	278	15.6	1.9	7.5	576
T2	119.9	123.7	809	97.9	97.5	280	14.3	2.3	7.7	576
T3	120.4	122.2	808	80.4	77.1	232	15.2	2.4	8.0	560
T4	121.4	124.0	808	60.7	63.1	166	14.0	2.0	7.7	540
T5	182.0	184.4	1168	90.5	92.7	262	16.3	1.4	7.4	750
T6	239.8	242.8	1529	120.6	122.2	349	15.0	2.1	7.5	960
T7	301.4	302.7	1891	151.3	152.1	441	15.4	1.7	7.3	1170

Table 2

Test results of fabricated HSS RHS T-joint specimens.

Specimen	β	2γ	f_y (MPa)	$3\%b_0$ (mm)	N_{Test} (kN)	N_{FE} (kN)	N_{CIDECT} (kN)	N_{FE}/N_{Test}	N_{CIDECT}/N_{Test}
T1	0.80	19.8	907	3.65	826	788	378	0.95	0.46
T2	0.82	19.5	907	3.60	841	846	408	1.01	0.48
T3	0.67	19.6	907	3.61	492	535	301	1.09	0.61
T4	0.50	19.8	907	3.64	333	313	228	0.94	0.69
T5	0.50	29.6	907	5.46	264	246	246	0.93	0.93
T6	0.50	39.1	907	7.19	226	203	254	0.90	1.13
T7	0.50	49.1	907	9.04	188	182	257	0.97	1.37
Mean								0.97	0.81
COV								0.063	0.425

Table 3

Effects of heat affected zones on fabricated S960 steel RHS T-joints.

FE specimen	b_0 (mm)	h_0 (mm)	t_0 (mm)	b_1 (mm)	h_1 (mm)	L_1 (mm)	L_s (mm)	β	2γ	N_{u1} (kN)	N_{u2} (kN)	N_{u2}/N_{u1}
T1	121.7	122.9	6.14	96.8	98.3	278	576	0.80	19.8	786	738	0.94
T1-1	121.7	122.9	6.14	121.7	122.9	360	600	1.00	19.8	1034	974	0.94
T4	121.4	124.0	6.14	60.7	63.1	166	540	0.50	19.8	314	275	0.88
T4-1	121.4	124.0	6.14	36.4	36.4	110	516	0.30	19.8	170	153	0.90
T5	182.0	184.4	6.14	90.5	92.7	262	750	0.50	29.6	246	212	0.86
T6	239.8	242.8	6.14	120.6	122.2	349	960	0.50	39.1	203	180	0.89

Note: N_{u1} and N_{u2} represent the joint strengths without and with HAZ, respectively.

Table 4

Material properties adopted for fabricated HSS RHS T-joints (Lan et al. [21]).

Steel grade	E (GPa)	f_y (MPa)	f_u (MPa)	ε_{sh} (%)	ε_u (%)
S460	206	460	550	2.00	14.0
S690	206	690	770	0.33	8.0
S960	206	960	980	0.47	5.5
S960-R10	206	864	882	0.42	5.5
S960-R20	206	768	784	0.37	11.6

Note: The value following the letter R denotes the percentage of material strength reduction; ε_{sh} is the strain-hardening strain.

Table 5

Series of fabricated RHS T-joints using S460, S690 and S960 steel for the parametric study.

Series No.	b_0 (mm)	h_0 (mm)	b_1 (mm)	h_1 (mm)	β	η	ζ	2γ
1	480	480	144	144	0.3	0.3	1.0	[15-40]
2	480	480	192	192	0.4	0.4	1.0	[15-40]
3	480	480	240	240	0.5	0.5	1.0	[15-40]
4	480	480	288	288	0.6	0.6	1.0	[15-40]
5	480	480	336	336	0.7	0.7	1.0	[15-40]
6	480	480	384	384	0.8	0.8	1.0	[15-40]
7	480	480	432	432	0.9	0.9	1.0	[15-40]
8	480	480	480	480	1.0	1.0	1.0	[15-40]
9	480	480	480	240	1.0	0.5	1.0	[15-40]
10	480	240	480	240	1.0	0.5	0.5	[15-40]

Table 6

Results of statistical analysis for fabricated HSS RHS T-joints.

Parameter	N_{CIDECT}/N_{FE}			$N_{Proposed}/N_{FE}$		
range	No. of data	Mean	COV	No. of data	Mean	COV
$0.3 \leq \beta \leq 0.85$	90	0.95	0.237	66	0.83	0.155
$0.85 < \beta < 1.0$	15	0.57	0.060	15	0.85	0.041
$\beta = 1.0$	40	0.44	0.601	40	0.89	0.168
Total	145	0.77	0.420	121	0.85	0.154

Table 7

Comparison of strength predictions with test strengths for chord side wall failure in cold-formed steel RHS T-joints with β=1.0.

Specimen	η	2γ	h_0/t_0	f_y (MPa)	N_{Test} (kN)	N_{CIDECT}/N_{Test}	$N_{Proposed}/N_{Test}$
TF-100x50x4-100x50x4 [17]	0.5	25	13	952	494	0.70	1.07
TF-120x120x4-120x120x4 [17]	1.0	31	31	971	558	0.32	1.02
TF-140x140x4-140x140x4 [17]	1.0	36	35	1008	544	0.30	1.03
TF-120x120x3-120x120x3 [17]	1.0	39	39	1038	369	0.26	0.92
S1B1C11 [37]	1.0	10	21	379	324	0.53	0.87
S1B1C12 [37]	1.0	16	32	373	163	0.35	0.98
S1B2C21 [37]	1.0	11	11	421	1193	0.88	1.00
S1B2C22 [37]	1.0	16	16	412	652	0.78	1.06
Mean						0.51	0.99
COV						0.442	0.067

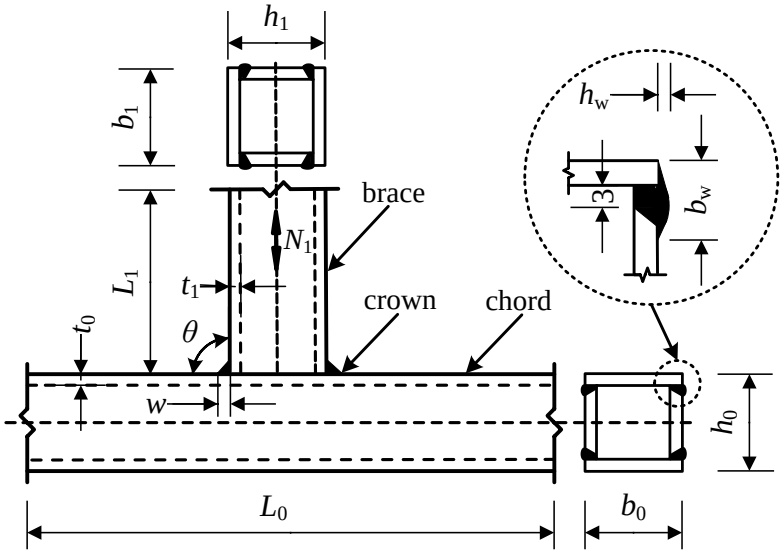

Fig. 1. Configuration and notations of fabricated RHS T-joints (dimensions in mm).

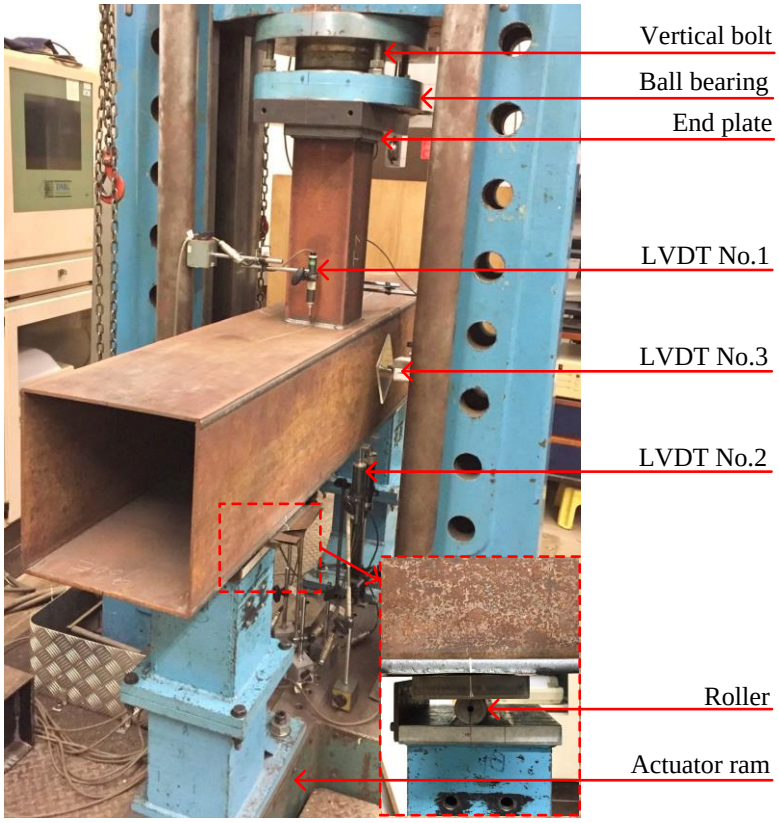

Fig. 2. Test set-up for fabricated HSS RHS T-joint specimens.

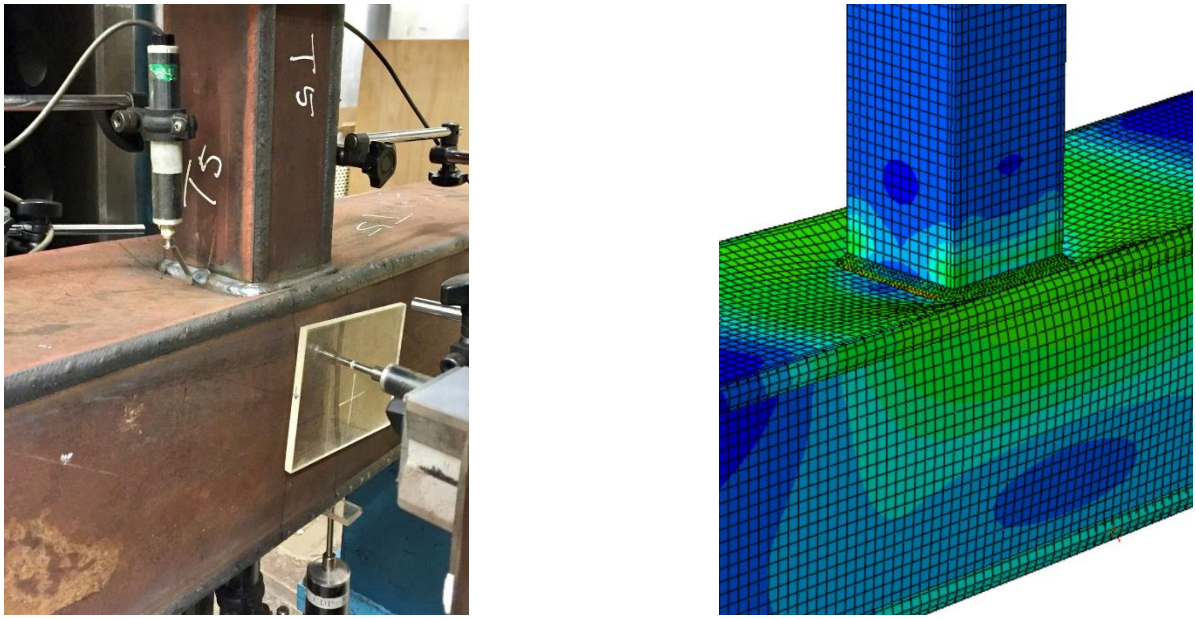

(a) Test observation (b) Numerical simulation

Fig. 3. Chord face plastification failure in the specimen T5.

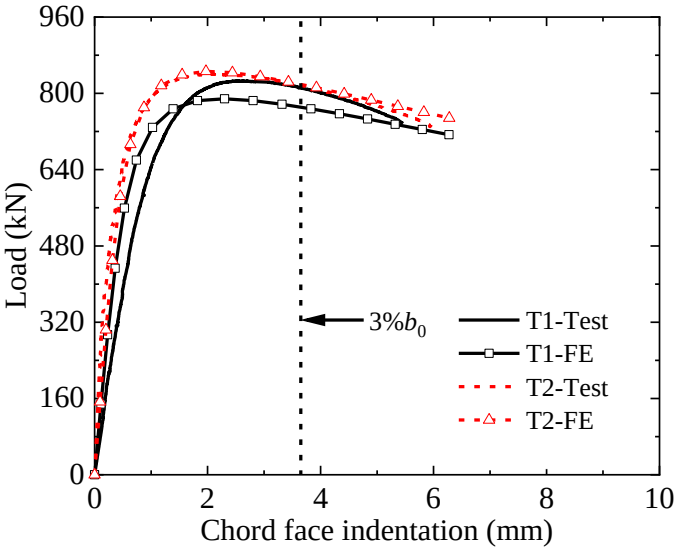

(a) Specimens T1 and T2

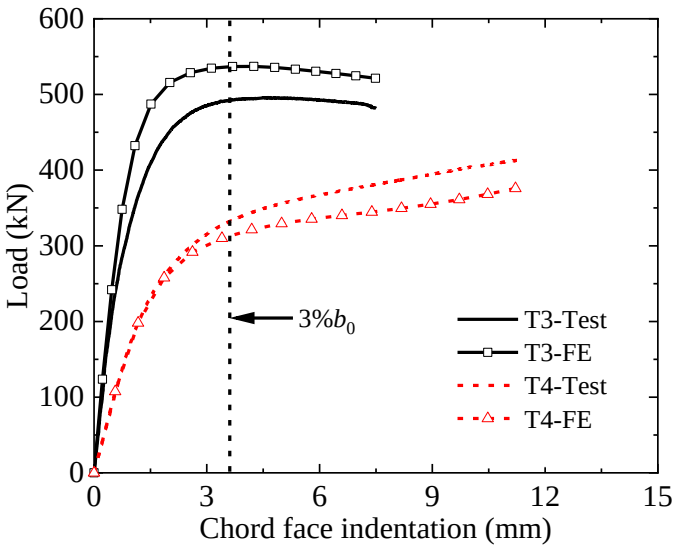

(b) Specimens T3 and T4

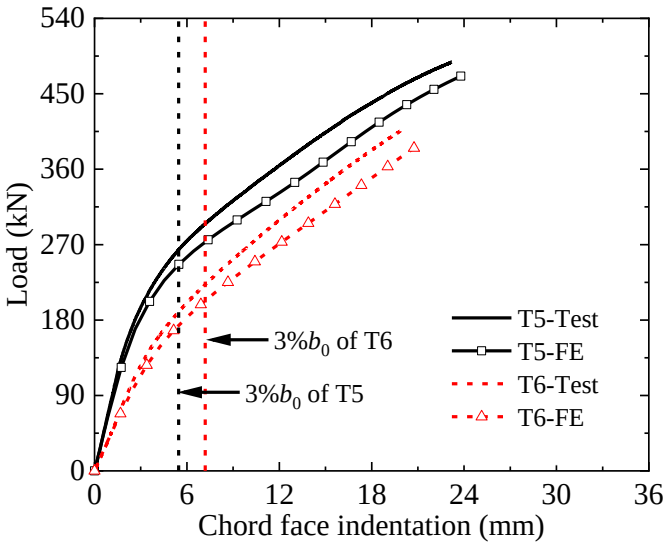

(c) Specimens T5 and T6

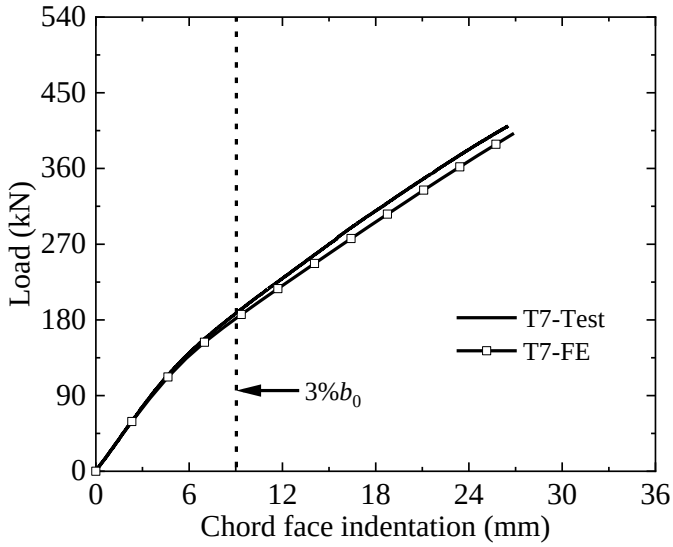

(d) Specimen T7

Fig. 4. Comparison of load-chord face indentation curves of HSS RHS T-joint specimens.

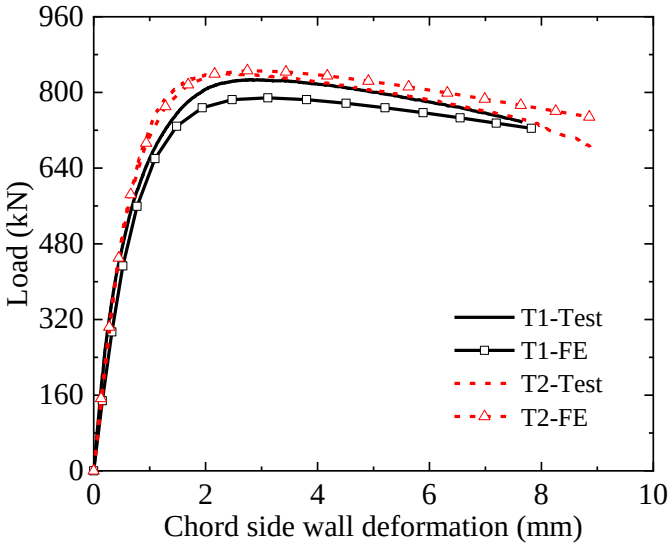

(a) Specimens T1 and T2

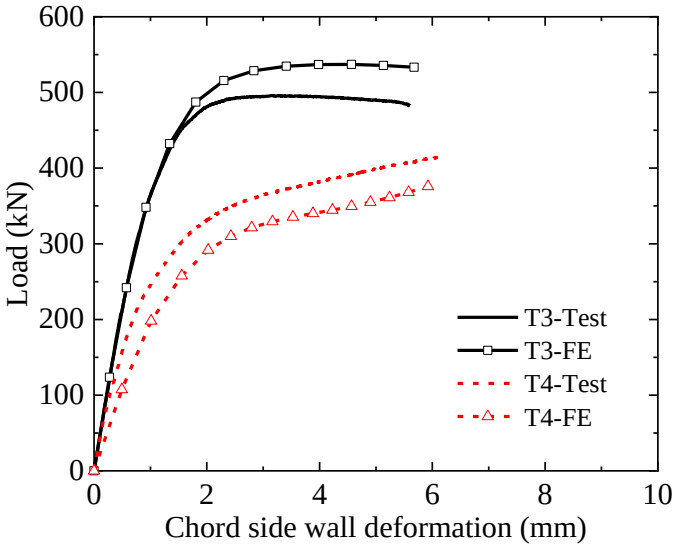

(b) Specimens T3 and T4

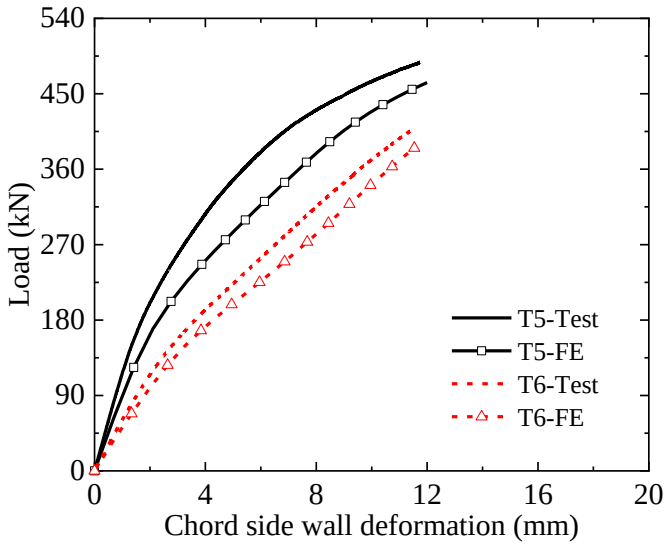

(c) Specimens T5 and T6

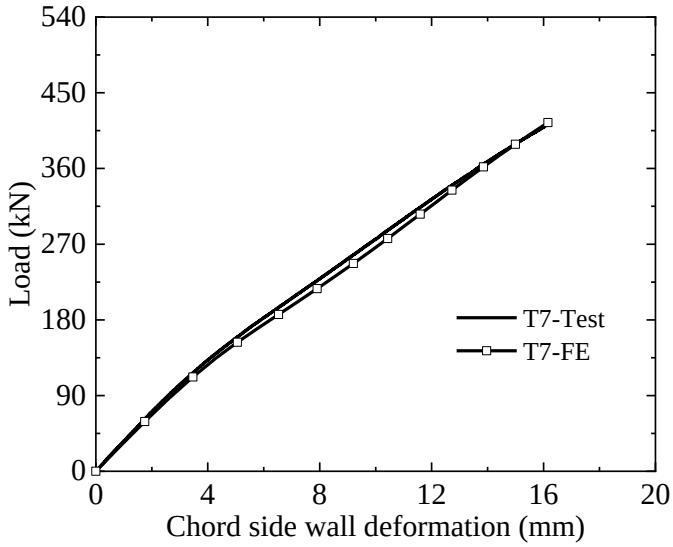

(d) Specimen T7

Fig. 5. Comparison of load-chord side wall deformation curves of HSS RHS T-joint specimens.

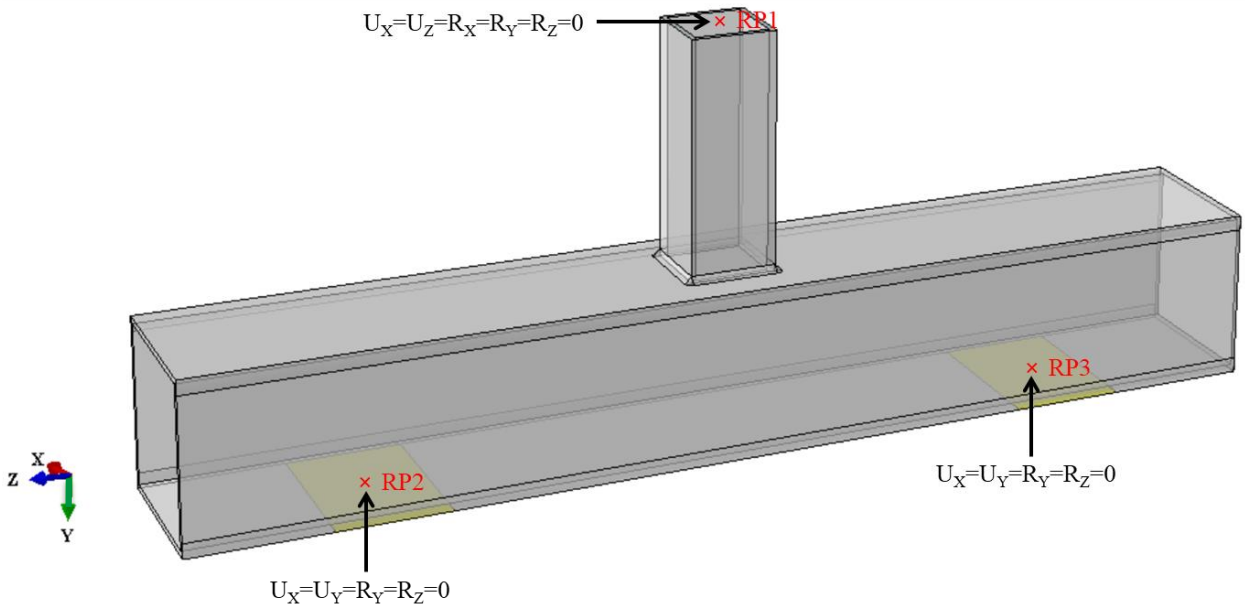

Fig. 6. Boundary conditions adopted for the FE model.

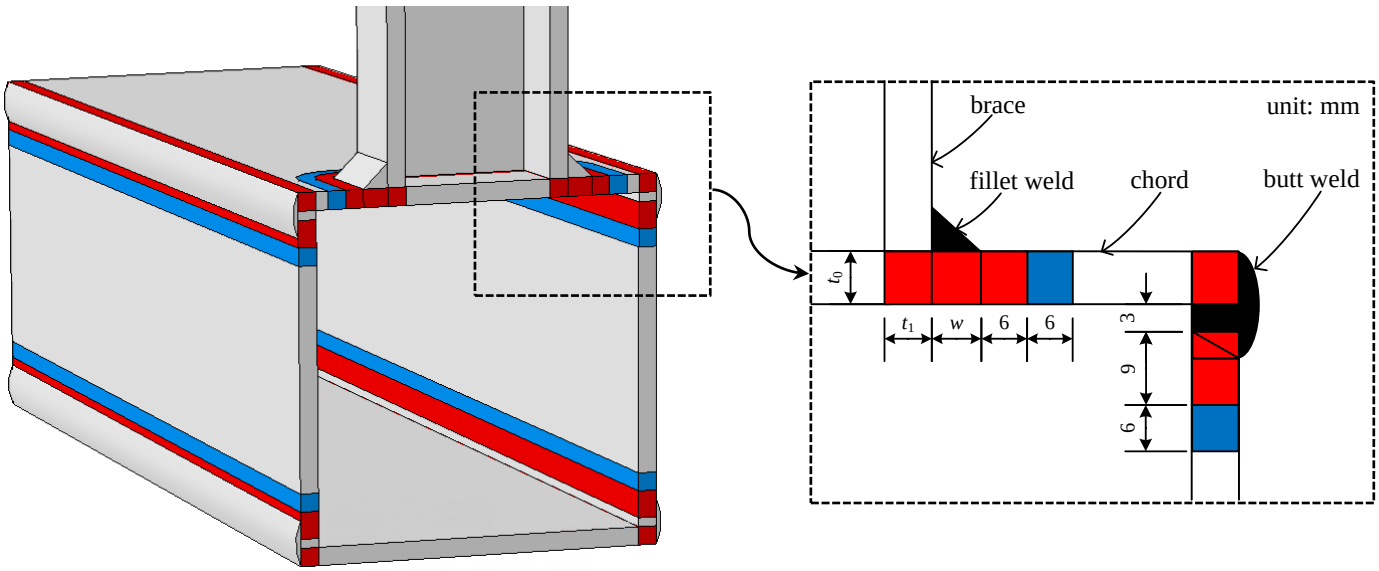

Fig. 7. Heat affected zones in S960 steel RHS T-joints (20% and 10% material softening in red and blue regions, respectively).

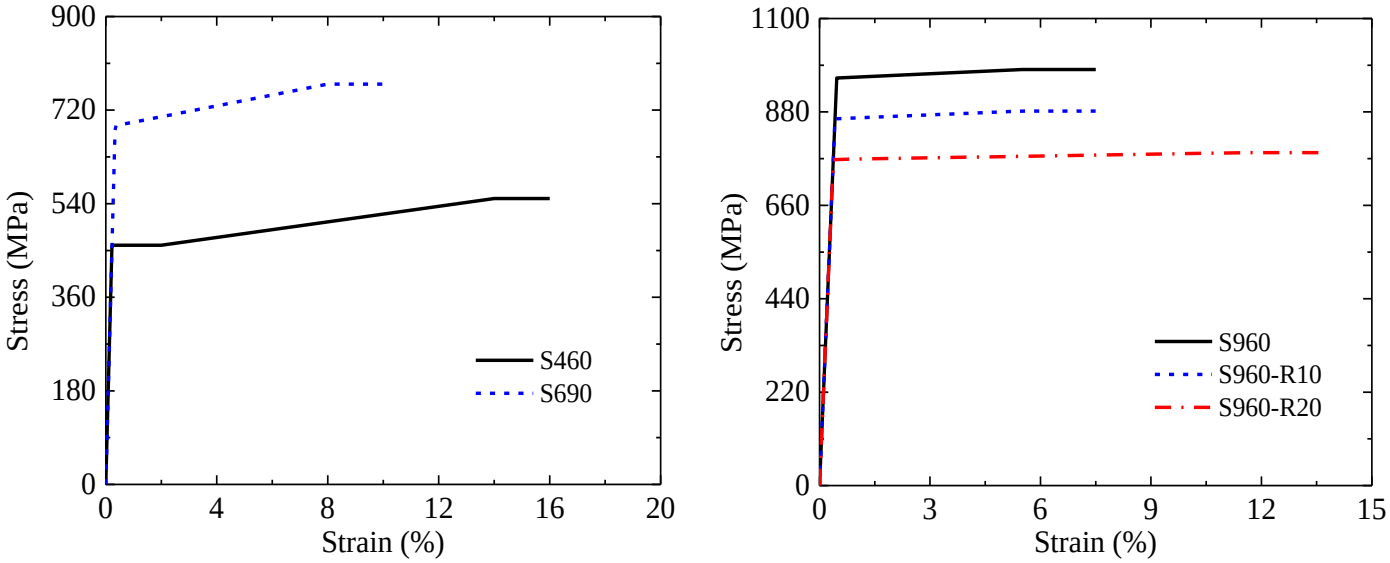

(a) S460 and S690

(b) S960

Fig. 8. Engineering stress-strain curves of HSS.

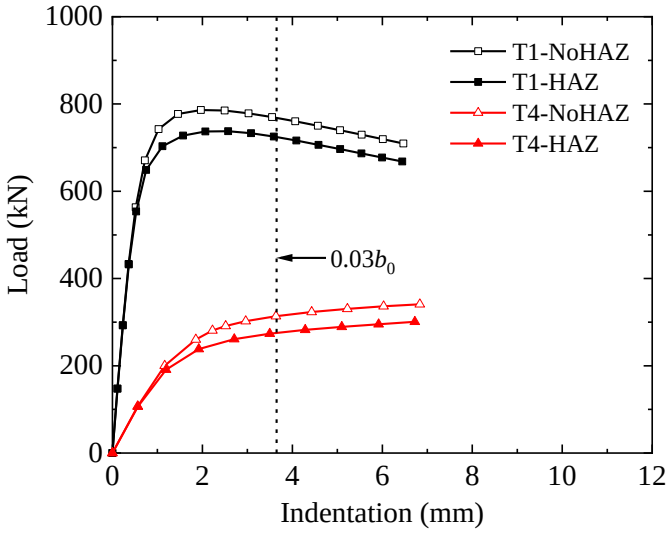

(a) FE specimens T1 and T4

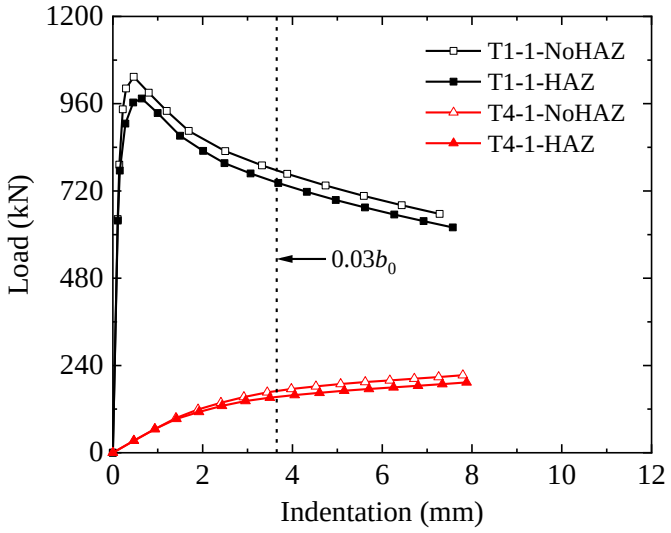

(b) FE specimens T1-1 and T4-1

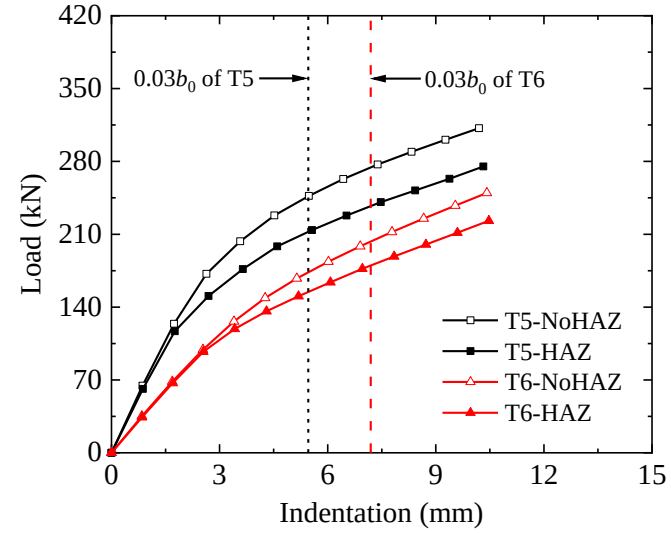

(c) FE specimens T5 and T6

Fig. 9. Load-indentation curves of S960 steel RHS T-joints without and with HAZ.

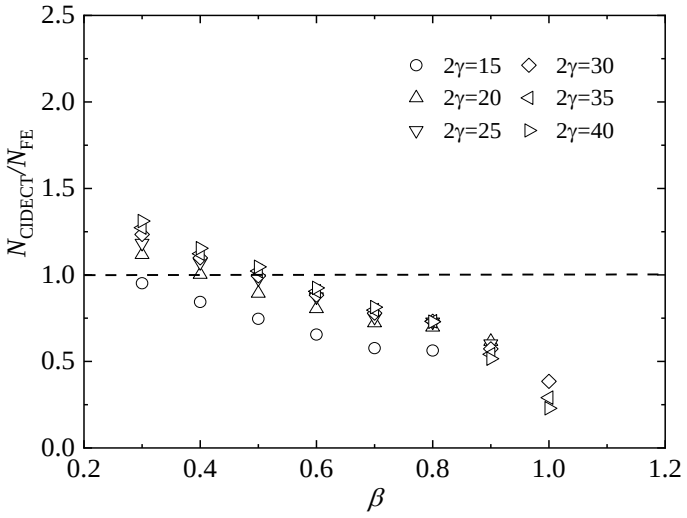

(a) S460

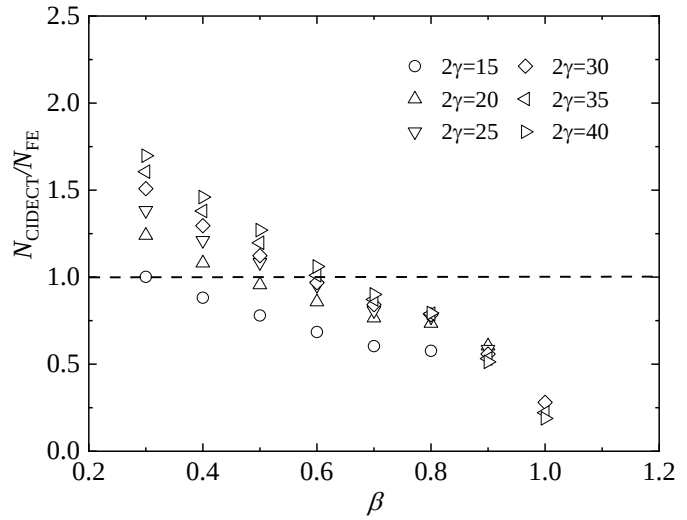

(b) S690

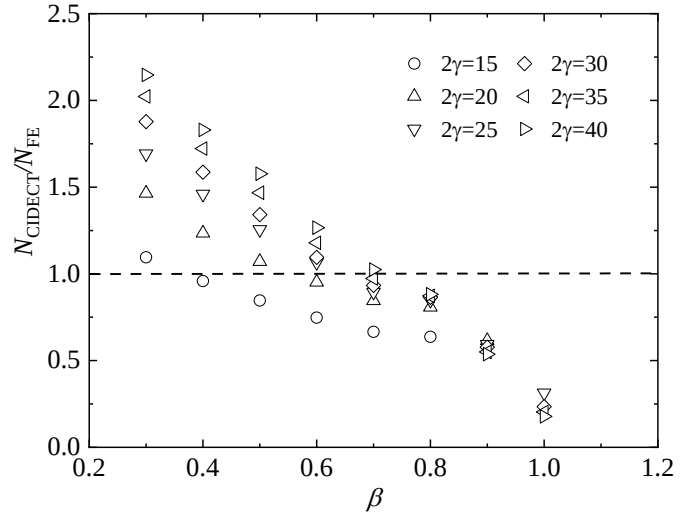

(c) S960

Fig. 10. Comparison of CIDECT strength prediction with FE strength for fabricated HSS RHS T-joints.

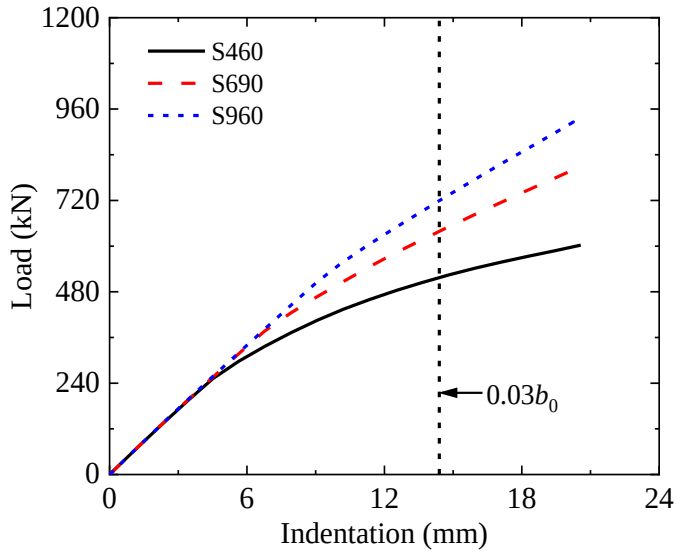

(a) β=0.3

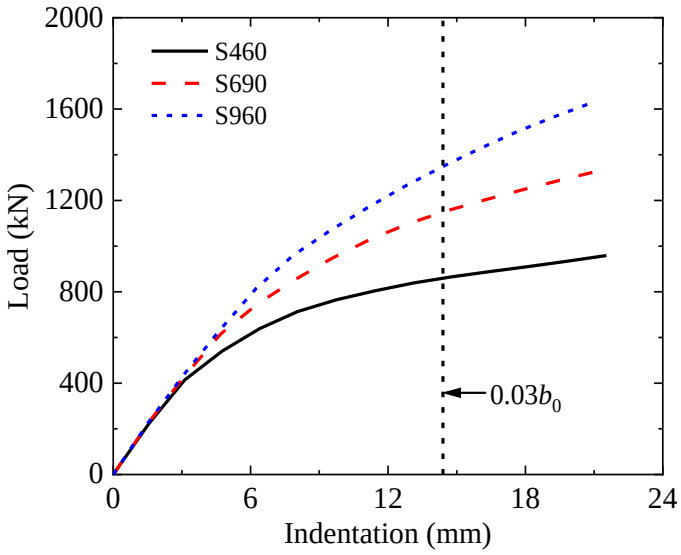

(b) β=0.5

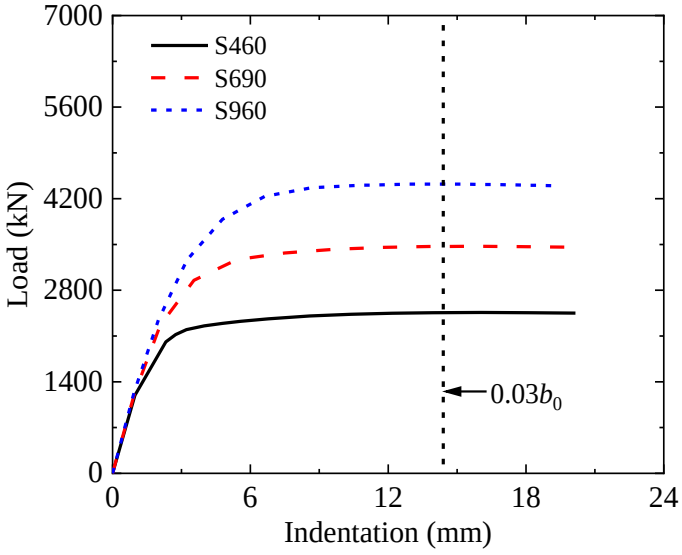

(c) β=0.8

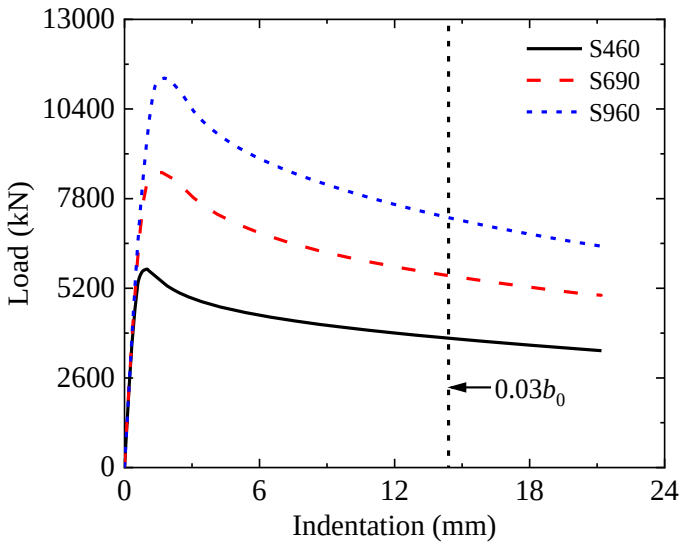

(d) β=1.0

Fig. 11. Typical load-indentation curves of fabricated RHS T-joints with 2γ=30.

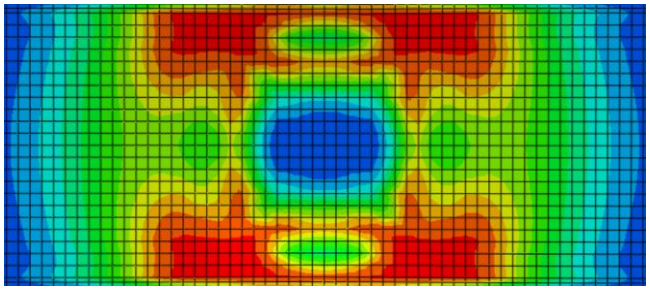

(a) S460

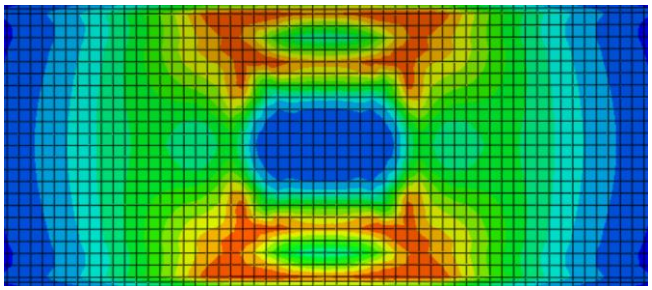

(b) S690

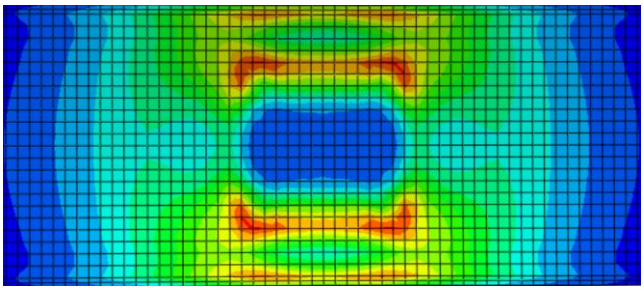

(c) S960

Fig. 12. Typical yielding patterns on chord faces of fabricated RHS T-joints with β=0.5 and 2γ=30.

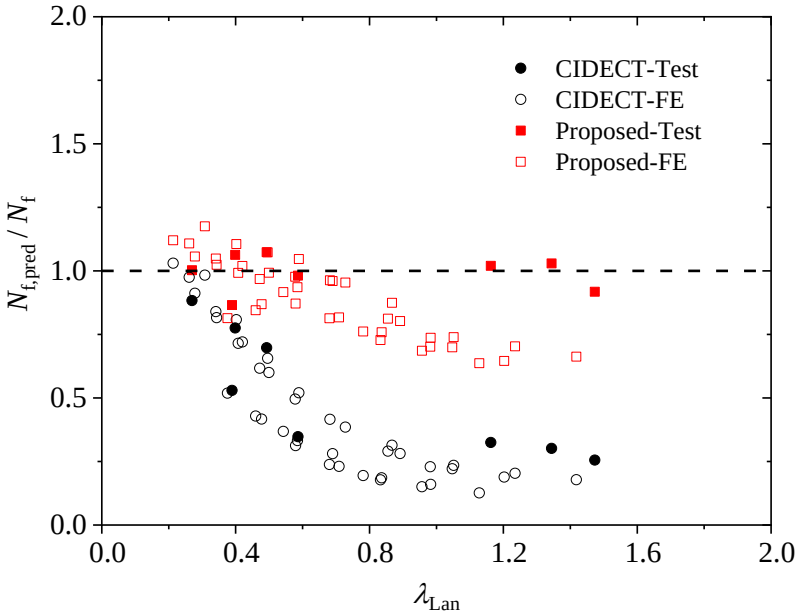

Fig. 13. Comparison of predicted strengths with test and FE strengths of RHS T-joints with β=1.0.